ADVANCED ENERGY MATERIALS

Postfach 10 11 61
69451 Weinheim
Germany
Courier services:
Boschstraße 12
69469 Weinheim
Germany
Tel.: (+49) 6201 606 235
Fax: (+49) 6201 606 500
E-mail: advenergymat@wiley-vch.de

WILEY-VCH

Dear Author,

Please correct your galley proofs carefully and return them no more than three days after the page proofs have been received.

If you have not used the PXE system before, please view the Tutorial before checking your proofs: http://wileypxe.aptaracorp.com/pxewileyvch/UserDocument/UserGuide/WileyPXE5_AuthorInstructions.pdf

Please note any queries that require your attention. These are indicated with red Qs in the pdf or highlighted as yellow queries in the "Edit" window.

Please pay particular close attention to the following, as no further corrections can be made once the article is published online:

- **Names** of all authors present and spelled correctly
- **Titles** of authors are correct (Prof. or Dr. only: please note, Prof. Dr. is not used in the journals)
- **Addresses of all authors** and **e-mail address of the corresponding author** are correct and up-to-date
- **Funding bodies** have been included and grant numbers are accurate
- The **Title** of the article is OK
- All **figures** are correctly included
- **Equations** are typeset correctly

Note that figure resolution in the PXE system is deliberately lower to reduce loading times. This will be optimized before the article is published online.

Please send any additional information, such as figures or other display items, to advenergymat@wiley-vch.de, and please also indicate this clearly in the PXE "Edit" window by inserting a comment using the query tool.

Reprints may be ordered by filling out the accompanying form.
Return the reprint order form by e-mail with the corrected proofs, to Wiley- VCH: **advenergymat@wiley-vch.de**

Please limit corrections to errors already in the text. Costs incurred for any further changes will be charged to the author, unless such changes have been agreed upon by the editor.

The editors reserve the right to publish your article without your corrections if the proofs do not arrive in time. Note that the author is liable for damages arising from incorrect statements, including misprints.

ADVANCED ENERGY MATERIALS

Reprint Order Form 2016
- please return with your proofs -

Editorial Office:

Wiley-VCH Verlag, Boschstrasse 12
69469 Weinheim, Germany

Tel.: (+49) 6201 606 531
Fax: (+49) 6201 606 500

E-mail: advenergymat@wiley-vch.de
http://www.advenergymat.de

Manuscript No. _____

Please send me and bill me for

☐ no. of **reprints** via ☐ airmail (+ 25 Euro) ☐ surface mail

☐ **high-resolution PDF file** (330 Euro).

My e-mail address:

_____

Please note: It is not permitted to present the PDF file on the internet or on company homepages

★**Special Offer**★ If you order 200 or more reprints you will get a PDF file for half price.

Information regarding VAT
Please note that from German sales tax point of view, the charge for **Reprints, Issues or Posters** is considered as **"supply of goods"** and therefore, in general, such delivery is a subject to German sales tax. However,this regulation has no impact on customers located outside of the European Union. Deliveries to customers outside the Community are automatically tax-exempt. Deliveries within the Community to institutional customers outside of Germany are exempted from the German tax (VAT) only if the customer provides the supplier with his/her VAT number. The VAT number (value added tax identification number) is a tax registration number used in the countries of the European Union to identify corporate entities doing business there. It starts with a country code (e.g. FR for France, GB for Great Britain) and follows by numbers.

Cover Posters

Posters are available of all the published covers and frontispieces in two sizes

☐ DIN A2 42 x 60 cm/ 17 x 24in (one copy: **39 Euro**)

☐ DIN A1 60 x 84 cm/ 24 x 33in (one copy: **49 Euro**)

Postage for shipping posters overseas by airmail:
+ 25 Euro

Postage for shipping posters within Europe by surface mail:
+ 15 Euro

Mail reprints / cover posters to:

_____
_____
_____
_____
_____

Invoice address:

_____
_____
_____
_____
_____

Date, Signature **Stamp**

VAT no.: _____
(institutes / companies in EU countries only)

Purchase Order No.: _____

Credit Card Payment

VISA, MasterCard, AMERICAN EXPRESS
Please use the Credit Card Token Generator located at the website below to create a token for secure payment. The token will be used instead of your credit card number.

Credit Card Token Generator:
https://www.wiley-vch.de/editorial_production/index.php

Please transfer your token number to the space below.

Credit Card Token Number:

Price list for reprints (The prices include mailing and handling charges. All Wiley-VCH prices are exclusive of VAT)

No. of pages	Price (in Euro) for orders of 50 copies	100 copies	150 copies	200 copies	300 copies	500 copies
1-4	345	395	425	445	548	752
5-8	490	573	608	636	784	1077
9-12	640	739	786	824	1016	1396
13-16	780	900	958	1004	1237	1701
17-20	930	1070	1138	1196	1489	2022
for every additional 4 pages	147	169	175	188	231	315

★ **Special Offer** ★ If you order 200 or more reprints you will get a PDF file for half price.

Wiley-VCH Verlag GmbH & Co. KGaA; Location of the Company: Weinheim;
Chairman of the Supervisory Board: Stephen Michael Smith,
Trade Register: Mannheim, HRB 432833, General Partner: John Wiley & Sons GmbH,
Location: Weinheim, Trade Register Mannheim, HRB 432296,
Managing Director: Sabine Steinbach

WILEY-VCH

Full Paper

xxxx

A. Y. Chang, Y.-J. Cho, K.-C. Chen, C.-W. Chen, A. Kinaci, B. T. Diroll, M. J. Wagner, M. K. Y. Chan, H.-W. Lin, R. D. Schaller* .....x–xx

Slow Organic-to-Inorganic Sub-Lattice Thermalization in Methylammonium Lead Halide Perovskites Observed by Ultrafast Photoluminescence

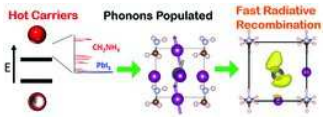

Ultrafast photoluminescence dynamics in $CH_3NH_3PbI_3$ perovskite thin films are examined as functions of pump wavelength, temperature, and film morphology. A previously unexplained, rapid decay feature in emission, which occurs only for above-gap excitation and lacks thermal activation, arises from organic-to-inorganic thermalization of phonons. Density functional theory and transient mid-infrared spectroscopy further support the assignment of this important dissipation mechanism.

aenm201600422(201600422)

www.advenergymat.de

ADVANCED ENERGY MATERIALS

Author Proof

Full Paper

Slow Organic-to-Inorganic Sub-Lattice Thermalization in Methylammonium Lead Halide Perovskites Observed by Ultrafast Photoluminescence

By *Angela Y. Chang, Yi-Ju Cho, Kuan-Chen Chen, Chang-Wen Chen, Alper Kinaci, Benjamin T. Diroll, Michael J. Wagner, Maria K. Y. Chan, Hao-Wu Lin, and Richard D. Schaller**

Keywords: density functional theory, perovskite, transient absorption, transient photoluminescence

ABSTRACT: Carrier dynamics in methylammonium lead halide ($CH_3NH_3PbI_{3-x}Cl_x$) perovskite thin films, of differing crystal morphology, are examined as functions of temperature and excitation wavelength. At room temperature, long-lived (>nanosecond) transient absorption signals indicate negligible carrier trapping. However, in measurements of ultrafast photoluminescence excited at 400 nm, a heretofore unexplained, large amplitude (50%–60%), 45 ps decay process is observed. This feature persists for temperatures down to the orthorhombic phase transition. Varying pump photon energy reveals that the fast, band-edge photoluminescence (PL) decay only appears for excitation ≥2.38 eV (520 nm), with larger amplitudes for higher pump energies. Lower photon-energy excitation yields slow dynamics consistent with negligible carrier trapping. Further, sub-band-gap two-photon pumping yields identical PL dynamics as direct absorption, signifying sensitivity to the total deposited energy and insensitivity to interfacial effects. Together with first principles electronic structure and ab initio molecular dynamics calculations, the results suggest the fast PL decay stems from excitation of high energy phonon modes associated with the organic sub-lattice that temporarily enhance wavefunction overlap within the inorganic component owing to atomic displacement, thereby transiently increasing the PL radiative rate during thermalization. Hence, the fast PL decay relates a characteristic organic-to-inorganic sub-lattice equilibration timescale at optoelectronic-relevant excitation energies.

1. Introduction

Methylammonium lead halide ($CH_3NH_3PbX_3$, X = Cl, Br, or I) perovskites have experienced a meteoric rise in the photovoltaic research field, with certified power conversion efficiencies that already exceed 20%.[1–3] Promising performance in light-emitting diodes[4–6] and lasers[7–10] has drawn still broader interest for optoelectronic applications. Improved understanding of the fundamental charge carrier interactions and dynamics occurring within this class of organic–inorganic perovskite can offer routes to further enhance both device efficiency and stability against degradation. To date, investigations into the charge carrier dynamics have revealed remarkable properties, including high carrier mobilities for a solution-processed semiconductor,[11–14] small carrier effective masses for both electrons and holes,[15–19] and long electron and hole diffusion lengths.[20–23] Transient absorption (TA) measurements indicate that carriers relax to the band-edge on a sub-picosecond timescale, and optical excitation results in dissociation of electron–hole pairs to yield free carriers.[21,24–27] Resultant radiative recombination occurs on a nanosecond timescale owing to nongeminate recombination, with faster decay rates at higher excitation fluence.[28] An examination of the vibrational dynamics of the organic moiety has suggested that methylammonium reorientation occurs

Dr. A. Y. Chang, M. J. Wagner, Prof. R. D. Schaller, Department of Chemistry, Northwestern University, 2145 Sheridan Rd Evanston, IL 60208, USA
Y.-J. Cho, K.-C. Chen, C.-W. Chen, Prof. H.-W. Lin, Department of Materials Science and Engineering, National Tsing-Hua University, Hsin Chu 30013, Taiwan
Dr. A. Kinaci, Dr. B. T. Diroll, Dr. M. K. Y. Chan, Prof. R. D. Schaller, Center for Nanoscale Materials, Argonne National Laboratory,, 9700 Cass Ave Argonne, IL 60439, USA
Correspondence to: Prof. R. D. Schaller (E-mail: schaller@anl.gov, schaller@northwestern.edu)
Q1
10.1002/aenm.201600422

 © 2016-05 WILEY-VCH Verlag GmbH & Co. KGaA, Weinheim

ADVANCED ENERGY MATERIALS

Author Proof

on an ≈3 ps timescale.[29] While the majority of photophysical research efforts have concentrated on room temperature behavior,[12,20,21,24,26,30–33] temperature-dependent studies provide additional insights,[12,13,19,28,34–44] especially with regard to energy landscapes and carrier fate.

The dissimilar masses of methylammonium and the Pb-I framework effectively comprise two largely independent sublattices with highly disparate vibrational frequencies,[45,46] with C–H and N–H stretching modes near 3000 cm^{-1} (≈0.37 eV) and Pb-I optical modes below 100 cm^{-1}.[47] For ambient and lower temperatures, the high frequency stretch modes corresponding to the organic molecules are not thermally populated, but may be optoelectronically relevant due to electron–phonon scattering. However, for $CH_3NH_3PbX_3$, interactions among excitons, charge carriers, and phonons, as well as the effects of such interactions on recombination dynamics, remain active topics of investigation.

Here, we examine the photophysics of $CH_3NH_3PbI_{3-x}Cl_x$ thin films using TA and ultrafast photoluminescence (uPL). At 298 K, using low-fluence 400 nm (3.1 eV) excitation, the dynamics of the long-lived TA band-edge bleach feature stand in contrast to uPL measurements, where the latter present a heretofore unexplained fast (≈45 ps) decay feature. To gain insight into the origin of this fast decay, we first vary temperature and note that the decay component clearly persists for the tetragonal phase, suggesting a lack of activated behavior. Below the phase transition temperature to orthorhombic near 150 K, the decay feature becomes obscured by interdomain energy transfer processes. Room temperature, low-fluence pump wavelength studies show that the amplitude of the fast decay feature becomes larger for higher energy photoexcitation. 2-photon excitation uPL measurements yield identical dynamics to 1-photon excitation, which relates a dependence on total energy deposited and a lack of interface-proximity effects. Further, mid-IR probing reveals a decay component that exhibits dependence on pump photon energies in similarity to the fast uPL decay feature. Based upon density functional theory (DFT) modeling, we interpret the fast PL decay as the timescale of diminishing electron–hole wavefunction overlap that results from equilibration of excited high frequency phonons in the organic sub-lattice with the low frequency inorganic sub-lattice following absorption of above-gap photons.

2. Results and Discussion

2.1. Significant Differences in Transient Absorption and Ultrafast Photoluminescence

Figure 1 compares spectrally and temporally resolved TA and uPL contour plots, generated from measurements using 400 nm pump excitation at 298 K and 1.7 μJ cm^{-2}, for a solution-processed $CH_3NH_3PbI_{3-x}Cl_x$ film. Immediately following photoexcitation, three well-studied spectral features appear in TA: a short-lived photoinduced absorption (PA) feature near 785 nm, a bleach maximum peaked at 756 nm (corresponding to a 1.64 eV band-gap), and a broad bleach shoulder around 680 nm (Figure 1a). At times longer than 2 ps, the PA and the bleach shoulder signals have decayed (with time constants of

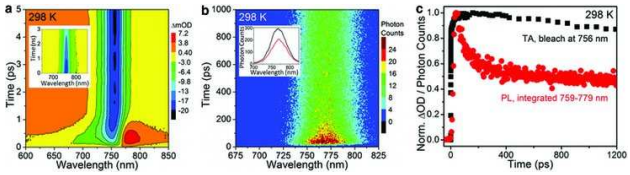

Figure 1. $CH_3NH_3PbI_{3-x}Cl_x$ thin film at 298 K excited at 400 nm with 1.7 μJ cm^{-2}. a) TA, for 5 ps and 3 ns (inset) timescales, shows slow dynamics following the initial sub-picosecond intraband carrier relaxation. Negligible carrier trapping is demonstrated in the bleach dynamics centered at 756 nm. b) A uPL contour plot for a 1 ns time window shows rapid initial emission followed by a slower decay. The inset displays time-resolved PL spectra from 0–60 ps (black line) and 600–660 ps (red line); the peak position remains unchanged with time. c) Comparison of TA and uPL dynamics suggests the rate of PL decreases with time despite an absence of carrier trapping.

516 ± 38 fs and 557 ± 73 fs, respectively), leaving mainly only the band-edge bleach peak, which persists to nanosecond timescales with little decay (see inset, the fitted decay constant is 6.0 ± 1.1 ns). The short-lived PA and broad bleach shoulder both relate ultrafast cooling of hot carriers from an initial high energy state to the lower energy and longer lived band-edge state, in agreement with previous reports for this excitation density (≈3.5 × 10^{17} cm^{-3}).[21,27,31] There have been multiple claims that $CH_3NH_3PbI_3$ exhibits similar electron and hole effective masses,[15–18,24,27] which suggests that both charge carriers should contribute almost equally to the observed TA signal owing to comparable population factors.[24] As such, the persistence of the main TA bleach feature on nanosecond timescales (Figure 1a, inset) indicates that neither band-edge carrier experiences significant trapping for this or other examined samples.

A uPL contour plot, shown as Figure 1b, depicts temporally and spectrally resolved PL intensity, and the inset shows time-resolved PL spectra at early and later times [integrated from 0–60 ps (black line) and 600–660 ps (red line), respectively]. The PL spectral profile, with an intensity maximum at 769 nm and Gaussian lineshape, does not change appreciably over this time range. Figure 1c compares both the TA bleach decay at 756 nm as well as the spectrally-integrated (759–779 nm) PL dynamics normalized at early time. Notably, uPL displays a rapid decay that is not reflected in the TA bleach dynamics. The fast PL decay occurs on a timescale of 48.5 ± 8.2 ps, with 50% total amplitude decrease by 1.2 ns, whereas the TA trace has only decayed to 86% of its initial amplitude for this same window. Given that TA and uPL were measured under the same conditions, the different dynamics suggest that the rate of radiative recombination decreases with time despite a fairly constant number of electrons and holes on the measured timescale; a series of additional measurements presented below further bolster this statement.

To verify the robustness of this dynamic feature, we performed several additional measurements. First, we examined uPL as a function of 400-nm pump fluence and found the time constant and amplitude to be fluence independent from 0.25 to 11 uJ cm^{-2} (see the Supporting Information, Figure

 © 2016-05 WILEY-VCH Verlag GmbH & Co. KGaA, Weinheim

Author Proof

S1). Second, while the results presented herein describe reproducible observations that were conducted for multiple solution-processed $CH_3NH_3PbI_{3-x}Cl_x$ thin films, we also performed measurements on vapor-deposited thin film samples, which exhibit markedly different morphology (≈5× smaller grain size and lower porosity for vapor-deposited; see both Chen et al.[48] and Figures S2 and S3, Supporting Information), and obtained roughly identical uPL results with regard to decay amplitude and time-constant (Figures S4–S6, Supporting Information). This sample invariance suggests both that the observed fast PL decay (i) is not related to coarse sample morphology, to which other types of studies have described sensitivity,[49,50] and (ii) is not related to extrinsic impurities or defects (since quantity and type would likely vary); excitation wavelength dependent studies presented in Section 2.3 further bear this out. Third, regarding potential impurities such as PbI_2, X-ray diffraction (XRD) of the measured films show highly crystalline films devoid of obvious contaminant (Figure S7, Supporting Information); we elaborate on this aspect further in Section 2.4. Fourth, rapid translation (≈4 cm s^{-1}) of the sample during data acquisition did not impact the fast decay amplitude or lifetime (Figure S8, Supporting Information), which suggests that effects such as local charge buildup in the photoexcited region does not yield the observed fast decay.

Several processes can potentially produce the time-dependent decrease in instantaneous radiative rate in the absence of fast trapping. Possibilities include (i) temperature-activated carrier trapping, (ii) free carrier diffusion of geminate electron–hole pairs, (iii) spin flips to yield triplet electron–hole pairs, or (iv) changes in wavefunction overlap owing to crystal lattice vibrations (phonons). Of these, spin flips seem unlikely as the timescale of this process is reported to be 1–7 ps at room temperature.[51] To investigate the origin and activation of the fast PL decay, we next present uPL measurements as a function of temperature.

2.2. Temperature Dependence of Photoluminescence Spectra and Dynamics: Lack of Activation

Figure 2 shows uPL contour plots (Figure 2a–c), with corresponding time-resolved PL spectra [for early (0–60 ps, black line) and later (600–660 ps, red line) times] shown as insets, and dynamics (Figure 2d–f) from 175–135 K. Upon cooling from 298 to 175 K, the static emission redshifts and spectrally narrows,[28,39] though for a given temperature in this range the time-resolved spectra exhibit a roughly constant center wavelength and spectral profile with time (Figure 2a). The time-resolved PL peak at 175 K shows mono-exponential decay with a time constant of 40.2 ± 5.4 ps (Figure 2d). Significant changes in the PL behavior occur around 150 K (Figure 2b,e). At this temperature, a PL feature at 747 nm appears immediately upon photoexcitation and then rapidly decays (blue circles), while the strong emission near 790 nm grows in and persists through the experimental time window (red squares). At 5 K (Figure 2c,f), the bluer peak shows larger initial signal than that at 150 K, however at later times the peak at 784 nm is more prominent. The fitted timescales are summarized in Table S1 (Supporting Information). For comparison across temperatures, PL spectra at early and later times (including more temperatures than

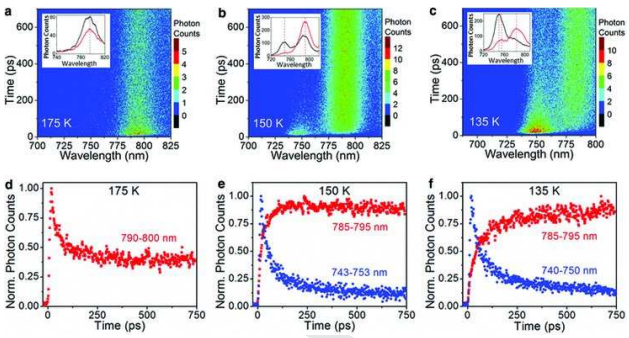

Figure 2. a–c) uPL contour maps and d–f) dynamics as a function of temperature and produced using low-fluence 400 nm excitation. Together these plots capture the spectral evolution that accompanies the phase transition from tetragonal to orthorhombic. a–c) Spectrally and temporally resolved uPL; insets show time-resolved spectra for early and late times [0–60 ps (black line) and 600–660 ps (red line), respectively], and vertical dashed lines indicate peak maxima. d–f) Normalized uPL dynamics, produced by integrating over the indicated wavelength ranges, from 175–135 K. d) Dynamics of the tetragonal phase at 175 K; similar behavior is observed between 298–175 K. e,f) The phase transition to orthorhombic occurs from 150–60 K, which is reflected in the dynamics through two distinct features: a high energy PL signal (blue circles), attributed to the orthorhombic phase, and a low energy PL signal (red squares), ascribed to the tetragonal phase.

shown in Figure 2) are shown in Figure S9 (Supporting Information).

The appearance and greater prominence of the higher energy emission occurring between 745–760 nm as temperature decreases is attributed to the emergence of the orthorhombic phase.[13,34] We observe that the phase transition from tetragonal to orthorhombic in this sample initiates near 150 K but is not entirely complete until near 60 K (Figure S10, Supporting Information). In this temperature range both phases coexist, with diminishing amounts of the tetragonal phase at lower temperatures. The polycrystalline form of this material and variation in crystallite size, defect density, and strain could potentially cause such phase coexistence.[28,36]

Upon the phase transition to orthorhombic, the fast PL decay feature is no longer clearly discernible due to energy transfer between the phases on a similar timescale. Since we are interested in understanding the origin of this fast PL feature, we return our focus to temperatures within the tetragonal phase (>160 K). For temperatures between 298 and 175 K, the fast PL decay feature maintains both comparable amplitude decay (50%–60%) and timescale (40–50 ps; Figures S11, Table S2 in the Supporting Information). This result indicates that processes such as activated carrier trapping or charge transfer do not give rise to the described PL decay feature, since the rate of such processes would scale as $e^{-1/T}$ (where T is temperature). Furthermore, the similarity of the decay amplitude and rate suggests that carrier mobility effects (such as geminate recombination) cannot explain the fast PL feature because this

 © 2016-05 WILEY-VCH Verlag GmbH & Co. KGaA, Weinheim

ADVANCED ENERGY MATERIALS

Author Proof

composition is reported to exhibit increased carrier mobility at lower temperatures,[12] which would lead to faster PL decays than are observed.

2.3. Pump Wavelength Dependence and Equilibration in Organic and Inorganic Sub-Lattices

Because varying temperature did not fully elucidate the origin of the fast PL feature, we investigated the influence of pump photon energy on PL dynamics at 298 K, as shown in **Figure 3**. Pump intensity and spot size were kept fairly constant for this measurement, and the traces were normalized to the signal level at 600 ps. For excitation at 690 and 550 nm (1.80 and 2.25 eV), only slow decay is observed on the measured timescale, which, consistent with TA, further supports that trapping of carriers at the band-edge is insignificant. At 520 nm, a fast component emerges in the dynamics that increases in amplitude with photon energy. By fixing the slow component of the decay to that obtained for 550 nm excitation (598 ± 253 ps), we arrive at time constants that systematically decrease from 69 to 41 ps for excitation at 520 to 350 nm (2.38 to 3.54 eV), respectively, with a corresponding increase in the decay amplitude (see also Table S3, Supporting Information). It is important to note that time-resolved PL spectra exhibit constant full-width at half-maximum (FWHM) for this full range of excitation wavelengths (see Figure S12 and Table S4 in the Supporting Information). The constant FWHM of time-resolved emission supports that bluer excitation does not cause new radiative relaxation from either impurities or from other optical transitions in the material. Also, blue versus red excitation does not yield any difference in measured uPL signal rise-time (here just limited by instrument response), which, again in agreement with TA, suggests that ultrafast relaxation into band-edge states dominates electronic relaxation.

Absorption coefficient for this composition does significantly increase with increasing photon energy, which causes absorption to occur with closer proximity for progressively bluer pump photons (≈300 nm penetration depth for our reddest excitation and ≈70 nm near 400 nm;[27] our samples were ≈300–450 nm thick). Indeed, Hsu et al. in ultrafast PL experiments exciting at 450 nm attributes observation of a tens-of-picosecond PL decay process, similar to what we observe, upon blue excitation by invoking relaxation into surface states.[32] To determine whether this fast PL feature might arise due to surface effects, we performed 2-photon excited uPL measurements. Whereas direct absorption suffers from the described penetration depth dictated by the inverse of the absorption coefficient, 2-photon absorption with sub-band-gap photons readily excites all the way through the studied films without depletion. As such, 2-photon excitation offers especially homogeneous electronic excitation through the depth of the studied films.[52] When comparing 1-photon and 2-photon measurements at 480 and 960 nm, respectively (Figure 3, inset), we obtain similar PL dynamics with regard to both decay amplitude and time constant, indicating that the fast PL decay process of interest does not result from surface effects and instead relates only to the total deposited photon energy.[52]

Recall that our results from temperature-dependent TA and uPL suggest that carrier trapping and carrier mobility do not

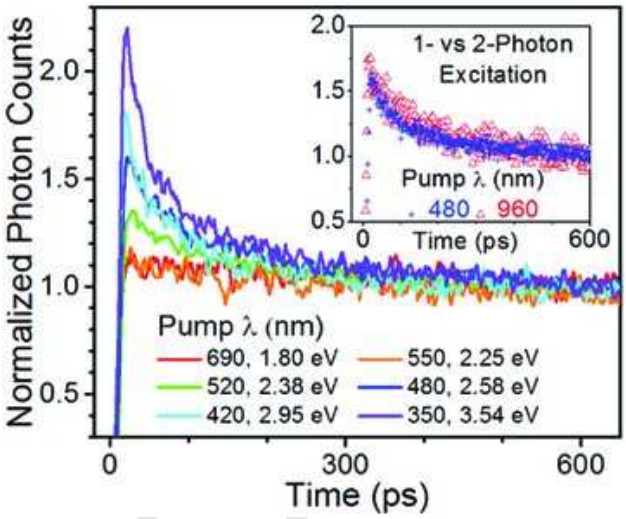

Figure 3. uPL dynamics obtained for indicated pump wavelengths at 298 K, normalized at 600 ps. A fast decay feature emerges for 520 nm pump, which becomes larger in amplitude for bluer wavelengths. Inset compares uPL dynamics measured for 1- and 2-photon excitation. These dynamics appear indistinguishable, indicating that the fast PL feature does not arise owing to surface effects.

offer satisfactory explanations for the observed fast PL feature with bluer pump wavelength. As such, we hypothesize that the initial high energy electron–hole pairs, created upon absorption of a sufficiently energetic photon, relax via scattering of high energy phonons, which involve and are indeed localized on the organic component of the perovskite rather than in the inorganic sub-lattice. We suggest that accessing the electronic states within these high energy ranges, via electron–phonon and phonon–phonon couplings, causes an increase in the spatial overlap of the carrier wavefunctions within the inorganic sub-lattice and thus results in increased instantaneous PL rate. Therefore, the timescale of the fast PL decay reflects the interconversion time of high frequency organic vibrations into low frequency inorganic modes. Mid-IR TA measurements probing at 3200 nm (≈0.39 eV, within the energy range that may emphasize the organic component), shown in **Figure 4**, lend support to this hypothesis. Excitation at 400 nm results in dynamics that at early time exhibit decay similar to the fast uPL decay. The dynamics from excitation at 600 nm lack this fast feature, instead displaying slow decay that also appears at later time (>150 ps) for 400 nm pump. Relatedly, we point out that Park et al., based on DFT calculations and Raman spectroscopy performed on $MAPbX_3$ perovskites invoked a similar model of photoexcitation wavelength-dependent dynamics that involves the organic sub-lattice.[53]

To understand how phonons can change the PL rate, we first establish the locations of charge density on this perovskite by performing DFT calculations at the generalized gradient approximation (GGA) level with spin–orbit coupling. Consistent with other reports,[15,16] we see that the valence band maximum (VBM) and conduction band minimum (CBM) states are

 © 2016-05 WILEY-VCH Verlag GmbH & Co. KGaA, Weinheim

Author Proof

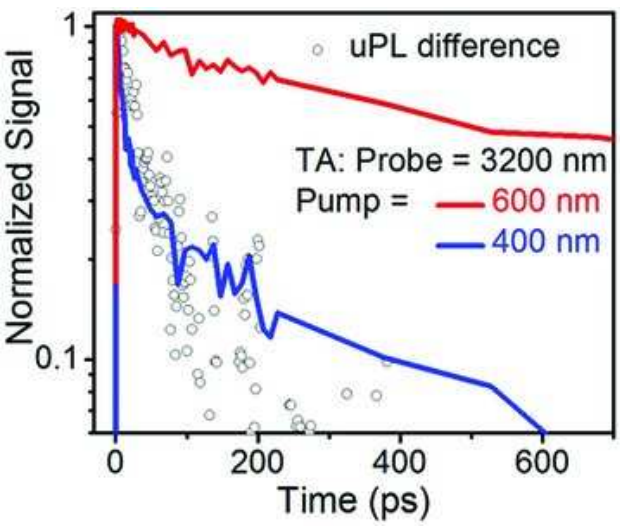

Figure 4. Normalized comparison of mid-IR TA signals (probe at 3200 nm), obtained using 400 nm (blue, 1.7 μJ cm^{-2}) and 600 nm (red, 6 μJ cm^{-2}) pump, against uPL data (open black circles), generated by taking the difference between the signals at 690 and 420 nm pump in order to isolate the fast PL decay feature. TA dynamics resulting from 400 nm excitation shows an initial rapid decay similar to the uPL feature, whereas the signal from 600 nm excitation decays more slowly.

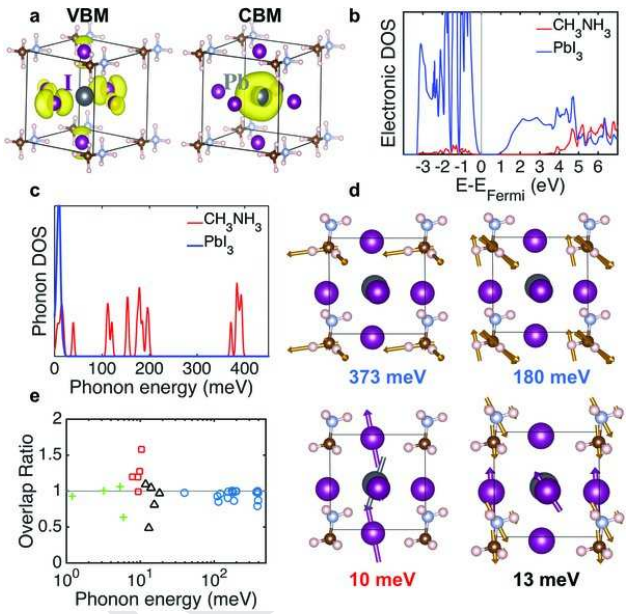

Figure 5. DFT-derived electronic and vibrational properties of $CH_3NH_3PbI_3$. a) Electronic charge density iso-surfaces of the valence band maximum (VBM) and conduction band minimum (CBM) states. Purple = I, gray = Pb, brown = C, blue = N, and pink = H. b) Electronic density of states decomposed by projections onto the organic (red) and inorganic (blue) sub-lattices. c) Phonon density of states decomposed by projections onto the organic (red) and inorganic (blue) sub-lattices. d) Examples of phonon modes at different frequencies. Lengths and directions of arrows represent magnitude and direction of motion of each atom within each phonon mode. e) Ratio of CBM–VBM orbital overlap for exciting each phonon mode, to the same overlap calculated when atoms are in the equilibrium position (i.e., without any phonon excitation), as a function of phonon energy.

highly localized on the Pb and I ions (**Figure 5**a). It follows that the overlap between those states, and therefore recombination rates, should be highly sensitive to the displacements of the Pb and I atoms. For methylammonium, the site-projected electronic density of states onto CH_3NH_3 does not become significant until the excitation energy exceeds ≈2–3 eV (Figure 5b), indicating that the organic molecules are not electronically excited by low-energy photons.

Next, we consider the distribution of phonons within this perovskite. The density of vibrational states obtained from the frozen phonon approach for both the organic and inorganic sub-lattices is shown in Figure 5c. As expected, the two sub-lattices present highly disparate vibrational frequencies, and the projection of vibrational modes above 200 cm^{-1} on the PbI_3 sub-lattice is approximately zero. The organic component possesses high-energy phonons from 100 to 400 meV (900–3200 cm^{-1}, 1300–4600 K), which are only accessible optoelectronically. In the 11–20 meV (90–150 cm^{-1}) range and below 6 meV (50 cm^{-1}), the phonon modes couple the organic and inorganic sub-lattices. Between 6–11 meV (50–90 cm^{-1}), phonon modes involve Pb and I, and are therefore expected to most significantly affect recombination. Examples of the different phonon modes are shown in Figure 5d. We introduce a small lattice distortion along the polarization vector of each phonon mode and calculate the induced changes in VBM–CBM wavefunction overlap (Figure 5e).[54] We find that the wavefunction overlap is significantly enhanced by exciting phonons in the 6–11 meV (50–90 cm^{-1}) range, by as much as 58% compared to the overlap without any phonon excitations.

Taken together with the electronic and phonon information calculated from DFT (Figure 5), the following sequence of events may explain the observed excitation-wavelength-dependent fast PL decay. High-energy photons excite the electronic states localized within the methylammonium molecules, which, via electron–phonon coupling within the molecules, create vibrations in otherwise unpopulated phonon modes (>100 meV). Phonon–phonon coupling to modes with energies between 6–11 meV, such as the ≈10 meV mode (Figure 5d), triggers enhanced radiative recombination. The characteristic timescale for this process is controlled by the phonon–phonon coupling of high-energy to low-energy phonons, or the transmission of vibrational energy from the organic to inorganic sub-lattice.

In order to obtain an estimate of the coupling timescale for vibrational modes between the two sub-lattices, we performed microcanonical (NVE) ab-initio molecular dynamics (AIMD) simulations starting with an excitation from the equilibrium position of the highest frequency modes (370–400 meV), which are entirely concentrated in the organic sub-lattice (Figure 5c). The equilibration of temperature serves as a proxy for the cou-

 © 2016-05 WILEY-VCH Verlag GmbH & Co. KGaA, Weinheim

pling time between these high-frequency modes and the remainder of the lattice. From a 50-ps AIMD trajectory, we obtain a decay time of 65 ps (76 ps) for a single exponential fit with (without) a constant term. These timescales are consistent with the experimentally observed tens-of-picosecond PL decay times.

2.4. Discussion of Results in the Context of Prior Reports

We note that multiple reports have examined this same material using differing optical excitation conditions, and here we attempt to briefly convey how the presented data and interpretation relates to some of these earlier formative studies. Xing et al.[21] measured TA of thin films comparing excitation at 400 and 600 nm. For both excitation conditions, intraband relaxation to the band-edge as denoted by bleach formation time (probing at 760 nm) displayed sub-picosecond carrier cooling with a ≈400 fs difference for the higher-energy excitation. Longer-time TA dynamics, out to 1.7 ns, presented by Xing in the same work showed fairly flat dynamics for both excitation conditions in close similarity to our findings. Based upon a small amplitude bleach feature near 480 nm that showed some ultrafast depopulation that correlated with the 400 fs cooling time into the band-edge upon higher energy excitation, Xing put forth the concept of a second, higher energy valence band (termed VB2), which participated in initial excitation and helped to explain the weak bleach feature. Using 387 nm excitation, Manser and Kamat[24] and Stamplecoskie et al.[26] also noted the VB2 higher energy bleach feature in TA and the latter report attributes this TA feature to charge transfer character derived from the lead and iodine in some similarity to photophysical studies of wide-gap PbI_2. Here, the authors offer that these higher energy states exhibit somewhat decoupled dynamics relative to the band-edge, but both the band-edge and VB2 feature were shown to decay substantially (up to 80%) over a 400 ps time window. The suggestion that a higher-energy state near 480 nm might be decoupled from the overall electronic density of states might convey that the herein presented results perhaps suffer from dynamics that relate some impurity absorption such as remnant PbI_2. Relatedly, Wang et al.[30] studied films in which they could observe by XRD the presence of substantial PbI_2 impurity and attributed a bleach feature at 510 nm (near VB2) to reflect bleaching of this impurity. In that work, band-edge TA bleach signals underwent fast and complete (near 100%) amplitude decay within a few hundred picoseconds.

As explained above, excitation of any impurities such as PbI_2, which by XRD we do not observe obvious signs of (Figure S7, Supporting Information), cannot explain our presented findings, and potential impact from a VB2 state is not directly manifest in our band-edge uPL measurements. Also, our electronic TA data show negligible band-edge decay regardless of excitation wavelength in similarity to Xing.[21] As noted above, our uPL data exhibit constant FWHM within noise that indicates a lack of any new spectral components contributing to the spectrally and temporally resolved PL (Figure S12, Supporting Information). Further, our uPL data do not exhibit a discernible rise feature for blue excitation; where rise features in instantaneous PL intensity could occur if effects such as energy transfer from potential excited impurities, like wide-gap PbI_2, to the perovskite occurred, and our excitation fluence (that is fluence independent over an order of magnitude) is sufficiently low that any form of high charge density-derived electronic processes can be ruled out. As stated before, the lack of fast band-edge PL decay for red optical excitation supports a lack of significant carrier trapping that is energetically downhill for band-edge carrier. Similarly, for blue excitation, note that the ≈45-ps fast PL decay feature is roughly two-orders of magnitude slower than intraband relaxation times for carriers to appear at the band-edge. For all of these reasons, we believe that impurities do not give rise to our long-lived TA and fast uPL decay, and the nature and origin of VB2 does not directly impact our measured signals.

On the other hand, we certainly expect that different initial charge density distributions do result from different pump photon energies, and indeed the mechanism that we put forth relies on the imparted excess energy whether derived from 1- or 2-photon excitation. Park et al.[53] conveyed through a combination of Raman spectroscopy and DFT modeling that increased involvement of the methylammonium ion with increasing pump photon excitation energy yields vibrational excitation of organic modes, which we further suggest impacts electron–hole wavefunction overlap as these dissimilar lattice frequencies of organic and inorganic equilibrate slowly in our picture. TA bleaching signals, because they are dominated by state-filling of absorbing transitions, do not noticeably change during this thermalization process.

Finally, we point out that at least two other time-resolved PL studies exhibit vestiges of the fast uPL decay feature we present here. The process we describe likely appears in the work by Bakulin et al.,[29] which primarily examined methylammonium reorientation dynamics using mid-infrared spectroscopy, but also described an additional tens-of-picosecond decay in the signal, consistent with the timescales we observe in mid-infrared TA and blue-excited uPL. Also, Hsu et al., exciting at 450 nm, observed several decay components, one of which we suggest we observe here, but whereas the decay component in that work suggested a surface effect, we ruled this out via 2-photon pumped PL with a sub-band-gap incident photon.

3. Conclusion

Through extensive comparisons of TA and uPL results for two different morphologies of polycrystalline thin films of $CH_3NH_3PbI_{3-x}Cl_x$, we showed that uPL exhibited rapid (≈45 ps) decay dynamics with large loss of signal amplitude (50% by ≈1 ns), in sharp contrast to slow carrier dynamics following the first picosecond seen in TA. Temperature-dependent uPL established that this fast feature persists with similar behavior through the tetragonal phase (298 to ≈150 K), however during the phase transition to orthorhombic (≈150 to ≈60 K), the fast feature becomes obscured as the dynamics of both phases complicate the electronic landscape. 1-photon photoexcitation-dependent studies demonstrated that the rapid PL decay became more prominent as pump photon energy increased, and the corresponding 2-photon measurements showed identical

 © 2016-05 WILEY-VCH Verlag GmbH & Co. KGaA, Weinheim

Author Proof

PL dynamics, signifying sensitivity to the total deposited excitation energy and insensitivity to potential interfacial effects. Additionally, mid-IR TA dynamics reproduced the fast PL decay for blue excitation. Density functional theory (DFT) calculations supported that despite the organic and inorganic sub-lattices having different vibrational frequencies, higher energy photons could excite electronic states that exhibit significant projections onto the organic sub-lattice, which in turn could excite high energy phonons in the same sub-lattice. During phonon–phonon coupling between sub-lattices, the recombination rates could be significantly affected due to altered orbital overlap. Thus, the ≈45 ps PL decay feature relates a characteristic organic-to-inorganic sub-lattice thermalization timescale.

The implications of sub-lattice equilibration, which affects the dynamics of band-edge carriers for solar-relevant wavelengths below 520 nm, can be substantial. For example, the material may become less stable because primarily the organic component (the more volatile of the two in this material) experiences elevated lattice temperature. Additionally, for laser applications, high frequency phonon populations should increase optical gain as wavefunction overlap increases.

Q2 4. Experimental Section

Film Preparation: A 40 nm PEDOT:PSS thin film was first coated on cleaned fused silica or IR transparent substrate by Q3 spin-coating. For solution-processed thin films, perovskite precursor solution was prepared by mixing the PbI_2, $PbCl_2$, and CH_3NH_3I in dimethylformamide solvent and coated on top of the PEDOT:PSS layer by spin-coating at 8000 rpm for 60 s. Then, the films were dried on a hot plate at 100 °C for 10 min.[55] The perovskite films prepared by vacuum sublimation were prepared by sequentially depositing $PbCl_2$ and CH_3NH_3I on PEDOT:PSS coated fused silica substrate in a vacuum chamber with base pressure of 10^{-6} Torr. The $PbCl_2$ converted into perovskite in situ in vacuum after evaporating CH_3NH_3I.[48] Scanning electron microscopy, atomic force microscopy, X-ray diffraction, and UV–vis data appear in Figures S1–S3 (Supporting Information). All thin film samples were ≈300–450 nm thick.

Transient Spectroscopy: Ultrafast photoluminescence and TA measurements were performed using a 35 fs amplified titanium:sapphire laser operating at 2 kHz. A time-delayed probe pulse was generated either from 800 nm pulses focused into a sapphire plate or from an optical parametric amplifier and was spatially overlapped with the pump. The pump excitation wavelength was generated using a separate optical parametric amplifier. Pump repetition rate was 2 kHz for uPL and 1 kHz for TA. uPL signal was collected using a single-photon sensitive streak camera that offers both temporally and spectrally resolved data. Samples were mounted on a sample in vacuum cryostat and maintained under 10^{-7} Torr vacuum.

Computational Methods: First principles DFT calculations were performed using the plane wave code Vienna Ab Initio Simulation Package (VASP),[56] with supplied projector augmented wave atomic potentials.[57] The GGA exchange correlation functional parameterized by Perdew, Burke, and Ernzerhof was used,[58] and spin–orbit coupling effects were included. The kinetic energy cutoff for the plane-wave basis was 500 eV. A 12-atom pseudo-cubic phase of $CH_3NH_3PbI_3$ was considered. A Γ-centered 6 × 6 × 6 k-point grid was used for Brillouin zone (BZ) sampling. The structure was relaxed until the forces on atoms were below 0.003 eV $Å^{-1}$. Vibrational frequencies were calculated using the frozen phonon approach with finite displacements of 0.01 Å. The Hessian matrix elements from the phonon calculation were used to generate full-BZ phonon dispersions using the PHONOPY code.[59] The reciprocal cell was represented by a Γ-centered 20 × 20 × 20 k-mesh, and the phonon density of states was calculated up to 110 THz within the sampled volume. A smearing width of 0.5 THz was selected for representing the phonon density of states in Figure 5a. The effects of vibrational modes on orbital overlap were investigated by performing static calculations of atomic configurations that were displaced from the equilibrium position by a fraction (0.1) of each of the phonon eigenvectors. Ab initio molecular dynamics simulations were carried out in VASP with the same parameters as total energy calculations, except with a 3 × 3 × 3 k-point grid. The time step was 0.5 fs. Atomic structures and charge density iso-surfaces in Figure 5c–d were produced using the visualization software VESTA.[60]

Supporting Information

Supporting Information is available from the Wiley Online Library or from the author.

Acknowledgements

This work was performed, in part, at the Center for Nanoscale Materials, a U.S. Department of Energy Office of Science User Facility under Contract No. DE-AC02-06CH11357. A.Y.C., B.T.D., M.J.W., and R.D.S. performed optical experiments. Y.J.C., K.C.C., C.W.C., and H.W.L. prepared and characterized the samples. A.K. and M.K.Y.C. performed electronic structure and dynamics calculations. The manuscript was written through contributions of all authors.

Received: February 25, 2016
Revised: April 7, 2016
Published Online: MM DD, YYYY

[1] C.-C. Chueh, C.-Z. Li, A. K.-Y. Jen, *Energy Environ. Sci.* **2015**, *8*, 1160.
[2] N.-G. Park, *Mater. Today* **2015**, *18*, 65.
[3] S. D. Stranks, P. K. Nayak, W. Zhang, T. Stergiopoulos, H. J. Snaith, *Angew. Chem. Int. Ed.* **2015**, *54*, 3240.
[4] Z.-K. Tan, R. S. Moghaddam, M. L. Lai, P. Docampo, R. Higler, F. Deschler, M. Price, A. Sadhanala, L. M. Pazos, D. Credgington, *Nat. Nanotechnol.* **2014**, *9*, 687.
[5] Y. H. Kim, H. Cho, J. H. Heo, T. S. Kim, N. Myoung, C. L. Lee, S. H. Im, T. W. Lee, *Adv. Mater.* **2015**, *27*, 1248.
[6] R. L. Z. Hoye, M. R. Chua, K. P. Musselman, G. R. Li, M. L. Lai, Z. K. Tan, N. C. Greenham, J. L. MacManus-Driscoll, R. H. Friend, D. Credgington, *Adv. Mater.* **2015**, *27*, 1414.

 © 2016-05 WILEY-VCH Verlag GmbH & Co. KGaA, Weinheim

[7] B. R. Sutherland, S. Hoogland, M. M. Adachi, C. T. O. Wong, E. H. Sargent, *ACS Nano* **2014**, *8*, 10947.
[8] F. Deschler, M. Price, S. Pathak, L. E. Klintberg, D.-D. Jarausch, R. Higler, S. Hu¨ttner, T. Leijtens, S. D. Stranks, H. J. Snaith, *J. Phys. Chem. Lett.* **2014**, *5*, 1421.
[9] K. Chen, A. J. Barker, F. L. Morgan, J. E. Halpert, J. M. Hodgkiss, *J. Phys. Chem. Lett.* **2014**, *6*, 153.
[10] G. Xing, N. Mathews, S. S. Lim, N. Yantara, X. Liu, D. Sabba, M. Grätzel, S. Mhaisalkar, T. C. Sum, *Nat. Mater.* **2014**, *13*, 476.
[11] C. S. Ponseca Jr., T. J. Savenije, M. Abdellah, K. Zheng, A. Yartsev, T. Pascher, T. Harlang, P. Chabera, T. Pullerits, A. Stepanov, J. P. Wolf, V. Sundstrom, *J. Am. Chem. Soc.* **2014**, *136*, 5189.
[12] T. J. Savenije, C. S. Ponseca, L. Kunneman, M. Abdellah, K. Zheng, Y. Tian, Q. Zhu, S. E. Canton, I. G. Scheblykin, T. Pullerits, A. Yartsev, V. Sundström, *J. Phys. Chem. Lett.* **2014**, *5*, 2189.
[13] C. C. Stoumpos, C. D. Malliakas, M. G. Kanatzidis, *Inorg. Chem.* **2013**, *52*, 9019.
[14] C. Wehrenfennig, G. E. Eperon, M. B. Johnston, H. J. Snaith, L. M. Herz, *Adv. Mater.* **2014**, *26*, 1584.
[15] J. M. Frost, K. T. Butler, F. Brivio, C. H. Hendon, M. van Schilfgaarde, A. Walsh, *Nano Lett.* **2014**, *14*, 2584.
[16] G. Giorgi, J.-I. Fujisawa, H. Segawa, K. Yamashita, *J. Phys. Chem. Lett.* **2013**, *4*, 4213.
[17] P. Umari, E. Mosconi, F. De Angelis, *Sci. Rep.* **2014**, *4*, 4467.
[18] W. J. Yin, T. Shi, Y. Yan, *Adv. Mater.* **2014**, *26*, 4653.
[19] A. Miyata, A. Mitioglu, P. Plochocka, O. Portugall, J. T.-W. Wang, S. D. Stranks, H. J. Snaith, R. J. Nicholas, *Nat. Phys.* **2015**, *11*, 582.
[20] S. D. Stranks, G. E. Eperon, G. Grancini, C. Menelaou, M. J. Alcocer, T. Leijtens, L. M. Herz, A. Petrozza, H. J. Snaith, *Science* **2013**, *342*, 341.
[21] G. Xing, N. Mathews, S. Sun, S. S. Lim, Y. M. Lam, M. Gratzel, S. Mhaisalkar, T. C. Sum, *Science* **2013**, *342*, 344.
[22] D. Shi, V. Adinolfi, R. Comin, M. Yuang, E. Alarousu, A. Buin, Y. Chen, S. Hoogland, A. Rothenberger, K. Katsiev, Y. Losovyj, X. Zhang, P. A. Dowben, O. F. Mohammed, E. H. Sargent, O. M. Bakr, *Science* **2015**, *347*, 519.
[23] Y. X. Zhao, A. M. Nardes, K. Zhu, *J. Phys. Chem. Lett.* **2014**, *5*, 490.
[24] J. S. Manser, P. V. Kamat, *Nat. Photonics* **2014**, *8*, 737.
[25] S. D. Stranks, V. M. Burlakov, T. Leijtens, J. M. Ball, A. Goriely, H. J. Snaith, *Phys. Rev. Appl.* **2014**, *2*.
Q4
[26] K. G. Stamplecoskie, J. S. Manser, P. V. Kamat, *Energy Environ. Sci.* **2015**, *8*, 208.
[27] Y. Yang, D. P. Ostrowski, R. M. France, K. Zhu, J. van de Lagemaat, J. M. Luther, M. C. Beard, *Nat. Photonics* **2016**, *10*, 53.
[28] C. Wehrenfennig, M. Liu, H. J. Snaith, M. B. Johnston, L. M. Herz, *APL Mater.* **2014**, *2*, 081513.
[29] A. A. Bakulin, O. Selig, H. J. Bakker, Y. L. Rezus, C. Mu¨ller, T. Glaser, R. Lovrincic, Z. Sun, Z. Chen, A. Walsh, *J. Phys. Chem. Lett.* **2015**, *6*, 3663.
[30] L. Wang, C. McCleese, A. Kovalsky, Y. Zhao, C. Burda, *J. Am. Chem. Soc.* **2014**, *136*, 12205.
[31] Y. Yamada, T. Nakamura, M. Endo, A. Wakamiya, Y. Kanemitsu, *J. Am. Chem. Soc.* **2014**, *136*, 11610.
[32] H. Y. Hsu, C. Y. Wang, A. Fathi, J. W. Shiu, C. C. Chung, P. S. Shen, T. F. Guo, P. Chen, Y. P. Lee, E. W. Diau, *Angew. Chem. Int. Ed.* **2014**, *53*, 9339.
[33] A. Marchioro, J. Teuscher, D. Friedrich, M. Kunst, R. van de Krol, T. Moehl, M. Gratzel, J.-E. Moser, *Nat. Photonics* **2014**, *8*, 250.
[34] T. Baikie, Y. Fang, J. M. Kadro, M. Schreyer, F. Wei, S. G. Mhaisalkar, M. Graetzel, T. J. White, *J. Mater. Chem. A* **2013**, *1*, 5628.
[35] V. D'Innocenzo, G. Grancini, M. J. Alcocer, A. R. Kandada, S. D. Stranks, M. M. Lee, G. Lanzani, H. J. Snaith, A. Petrozza, *Nat. Commun.* **2014**, *5*, 3586.
[36] H.-H. Fang, R. Raissa, M. Abdu-Aguye, S. Adjokatse, G. R. Blake, J. Even, M. A. Loi, *Adv. Funct. Mater.* **2015**, *25*, 2378.
[37] H. Oga, A. Saeki, Y. Ogomi, S. Hayase, S. Seki, *J. Am. Chem. Soc.* **2014**, *136*, 13818.
[38] M. Saba, M. Cadelano, D. Marongiu, F. Chen, V. Sarritzu, N. Sestu, C. Figus, M. Aresti, R. Piras, A. G. Lehmann, C. Cannas, A. Musinu, F. Quochi, A. Mura, G. Bongiovanni, *Nat. Commun.* **2014**, *5*, 5049.
[39] K. Wu, B. Ashok, C. Ma, Y. Du, Y. Yang, L. Li, T. Wu, *Phys. Chem. Chem. Phys.* **2014**, *16*, 22476.
[40] Y. Yamada, T. Nakamura, M. Endo, A. Wakamiya, Y. Kanemitsu, *IEEE J. Photovolt.* **2015**, *5*, 401.
[41] W. G. Kong, Z. Y. Ye, Z. Qi, B. P. Zhang, M. Wang, A. Rahimi-Iman, H. Z. Wu, *Phys. Chem. Chem. Phys.* **2015**, *17*, 16405.
[42] R. L. Milot, G. E. Eperon, H. J. Snaith, M. B. Johnston, L. M. Herz, *Adv. Funct. Mater.* **2015**, *25*, 6218.
[43] C. La-o-vorakiat, T. Salim, J. Kadro, M.-T. Khuc, R. Haselsberger, L. Cheng, H. Xia, G. G. Gurzadyan, H. Su, Y. M. Lam, R. A. Marcus, M.-E. Michel-Beyerle, E. E. M. Chia, *Nat. Commun.* **2015**, *6*, 8903.
[44] H. Wang, L. Whittaker-Brooks, G. R. Fleming, *J. Phys. Chem. C* **2015**, *119*, 19590.
[45] N. Onoda-Yamamuro, T. Matsuo, H. Suga, *J. Phys. Chem. Sol.* **1990**, *51*, 1383.
[46] C. Quarti, G. Grancini, E. Mosconi, P. Bruno, J. M. Ball, M. M. Lee, H. J. Snaith, A. Petrozza, F. D. Angelis, *J. Phys. Chem. Lett.* **2014**, *5*, 279.
[47] B. Winkler, M. Dove, E. Salje, M. Leslie, B. Palosz, *J. Phys.: Condens. Matter* **1991**, *3*, 539.
[48] C.-W. Chen, H.-W. Kang, S.-Y. Hsiao, P.-F. Yang, K.-M. Chiang, H.-W. Lin, *Adv. Mater.* **2014**, *26*, 6647.
[49] C. Zhang, D. Sun, C. X. Sheng, Y. X. Zhai, K. Mielczarek, A. Zakhidov, Z. V. Vardeny, *Nat. Phys.* **2015**, *11*, 428.
[50] Y. X. Tian, A. Merdasa, E. Unger, M. Abdellah, K. B. Zheng, S. McKibbin, A. Mikkelsen, T. Pullerits, A. Yartsev, V. Sundstrom, I. G. Scheblykin, *J. Phys. Chem. Lett.* **2015**, *6*, 4171.
[51] D. Giovanni, H. Ma, J. Chua, M. Grätzel, R. Ramesh, S. Mhaisalkar, N. Mathews, T. C. Sum, *Nano Lett.* **2015**, *15*, 1553.
[52] Y. Yamada, T. Yamada, P. Le Quang, N. Maruyama, H. Nishimura, A. Wakamiya, Y. Murata, Y. Kanemitsu, *J. Am. Chem. Soc.* **2015**, *137*, 10456.
[53] B. W. Park, S. M. Jain, X. L. Zhang, A. Hagfeldt, G. Boschloo, T. Edvinsson, *ACS Nano* **2015**, *9*, 2088.
[54] J. Ma, L.-W. Wang, *Nano Lett.* **2015**, *15*, 248.
[55] Y.-C. Huang, C.-S. Tsao, Y.-J. Cho, K.-C. Chen, K.-M. Chiang, S.-Y. Hsiao, C.-W. Chen, C.-J. Su, U. S. Jeng, H.-W. Lin, *Sci. Rep.* **2015**, *5*, 13657.
[56] G. Kresse, J. Furthmuller, *Comput. Mater. Sci.* **1996**, *6*, 15.
[57] G. Kresse, D. Joubert, *Phys. Rev. B* **1999**, *59*, 1758.
[58] J. P. Perdew, K. Burke, M. Ernzerhof, *Phys. Rev. Lett.* **1996**, *77*, 3865.
[59] A. Togo, F. Oba, I. Tanaka, *Phys. Rev. B* **2008**, *78*, 9.
[60] K. Momma, F. Izumi, *J. Appl. Crystallogr.* **2011**, *44*, 1272.

WILEY-VCH

 © 2016-05 WILEY-VCH Verlag GmbH & Co. KGaA, Weinheim

Q1 APT to AU: Please provide the highest academic title (either Dr. or Prof.) for all authors, where applicable.

Q2 APT to AU: The section heading 'Experimental Method' has been changed to Experimental Section. Please verify the change for correctness.

Q3 APT to AU: Please define PEDOT:PSS and PHONOPY at the first occurrence in the text.

Q4 APT to AU: Please provide page number in ref. (25).